

## Dynamics of High-Z Plasmas Produced by a Short-Wavelength Laser

P. D. Goldstone, S. R. Goldman, W. C. Mead, J. A. Cobble, G. Stradling, R. H. Day, and A. Hauer  
*Los Alamos National Laboratory, University of California, Los Alamos, New Mexico 87545*

and

M. C. Richardson, R. S. Marjoribanks, P. A. Jaanimagi, R. L. Keck, F. J. Marshall, W. Seka,  
 O. Barnouin, B. Yaakobi, and S. A. Letzring

*Laboratory for Laser Energetics, University of Rochester, Rochester, New York 14623*

(Received 25 August 1986)

The dynamics and energy flow in Au plasmas produced by a 0.35- $\mu\text{m}$  laser have been studied with layered targets with 6- and 24-beam spherical illumination from the Omega laser, to understand the processes leading to subkiloelectronvolt x-ray emission. A significant enhancement in x-ray conversion at low intensities is observed for the 24-beam irradiations with higher energy, greater uniformity, and larger targets. Results are interpreted by comparison with hydrodynamics-code calculations. The depth of energy penetration and x-ray emission in the plasma appears to be well understood, but some details of the x-ray time signature and spectra are not.

PACS numbers: 52.40.Nk, 32.30.Rj, 52.25.Nr, 52.50.Jm

The efficiency with which energy absorbed in laser-produced high-Z plasmas is converted to soft x rays increases markedly at shorter laser wavelengths.<sup>1-3</sup> This results from laser-light deposition at higher plasma densities, yielding cooler plasmas with lower hydrodynamic losses, and can be important for some approaches to inertial-confinement fusion.<sup>4</sup> A similar increase in conversion efficiency is expected at lower laser intensities. However, early experiments with planar Au targets<sup>1,2</sup> showed a decrease of x-ray emission at low intensities, whereas the LASNEX<sup>5</sup> simulations code predicted an increase,<sup>2</sup> indicating that high-Z plasmas were not well understood. Thus we have sought more specific observations of the hydrodynamic, energy-transport, and atomic processes which affect x-ray emission.

Here, we report the first measurements of x-ray conversion performed in spherical geometry. This pseudo one-dimensional experiment simplifies integration of measurements over solid angle and allows a test of whether two-dimensionality inherent in previous planar experiments might have affected the results.<sup>6,7</sup> Also, we examine the dynamics of high-Z plasmas and the processes which affect x-ray emission, including the material depths associated with energy transport and x-ray generation, and the time dependence and spectra of the x-ray emission, at intensities of  $4 \times 10^{12}$  to  $4 \times 10^{15}$  W/cm<sup>2</sup>. Finally, we compare similar experiments using two different laser-energy-target-size combinations at the  $4 \times 10^{13}$  and  $4 \times 10^{14}$  W/cm<sup>2</sup> intensities.

We have investigated some of the changes in plasma conditions which are expected as the  $\lambda_L = 0.35 \mu\text{m}$  irradiance is decreased from  $4 \times 10^{14}$  to  $4 \times 10^{13}$  W/cm<sup>2</sup> (where the emission discrepancy was first noted<sup>2</sup>). At  $4 \times 10^{14}$  W/cm<sup>2</sup>, radiation cooling is weaker than laser deposition in the underdense plasma. Hence the corona

temperature rises, reducing the inverse-bremsstrahlung absorption opacity, so that the laser penetrates to the critical surface and deposits its energy locally. This produces strong steepening of the density and temperature profiles near the critical density. The x-ray emission originates in a localized region near and above the critical density, with electron transport carrying energy from the absorption region to the emitting region. At  $4 \times 10^{13}$  W/cm<sup>2</sup>, radiation cools the corona at a rate nearly equal to the laser deposition, so that the deposition and the x-ray emission occur in an extended plasma well below the critical density. Electron transport is relatively unimportant in this case.

Specific predictions of the features of the x-ray-emission region are shown in Table I. The one-dimensional (1D) LASNEX<sup>5</sup> modeling used for this work

TABLE I. Calculated ( $f_e = 0.08$ ,  $\lambda_L = 0.35$ ,  $\tau_L = 650$  ps) characteristics of the subkiloelectronvolt x-ray emission and burnthrough features for layered Au-on-(CH)<sub>x</sub> spheres.

	$4 \times 10^{13}$ W/cm <sup>2</sup>	$4 \times 10^{14}$ W/cm <sup>2</sup>
X-ray emission		
Radial extent ( $\mu\text{m}$ )	40	8
Density	$(0.04-0.5)n_c$	$(0.3-1.8)n_c$
Electron temperature (keV)	0.1-0.5	0.3-1.2
Average Z	25-30	35-45
$E_{\text{rad}}/E_{\text{abs}}$	0.85	0.72
$E_{\text{M lines}}/E_{\text{rad}}$ (%)	<1	5
Burnthrough features		
Laser penetration depth (at peak of pulse) ( $\text{\AA}$ )	350	750
X-ray-emission decrease (at burnthrough)	Negligible	Significant

includes inverse bremsstrahlung laser deposition, Lagrangean hydrodynamics, thermal electron diffusion with flux limit of  $f_e = 0.03$  (as in previous work<sup>2</sup>) or 0.08 (best fit for this and related low- $Z$  spherical<sup>7</sup> work), and multigroup flux-limited x-ray diffusion. The modeling includes non-local-thermodynamic-equilibrium atomic and radiation physics, with a time-dependent solution of the average-atom hydrogenic collisional and radiative rate equations, neglecting subshell energy splittings and transitions. It closely corresponds with that used previously,<sup>2,7,8</sup> except for the omission of suprathermal electrons. Related 2D calculations including ray-trace modeling of the laser beams (we use tangential force but with axisymmetry) gave nearly identical results.

With use of layered Au-on-(CH)<sub>x</sub> targets, the penetration of energy through the Au into the (CH)<sub>x</sub> (burnthrough) can be observed by detection of changes in the emission when (CH)<sub>x</sub> replaces Au in the x-ray-emitting plasma, since the low- $Z$  (CH)<sub>x</sub> is a poor emitter. The Au thickness penetrated by the laser decreases as the intensity decreases (Table I). Furthermore, the effect of burnthrough on emission varies with intensity. At  $4 \times 10^{14}$  W/cm<sup>2</sup>, an abrupt reduction in low-energy x-ray flux is expected when the laser burns through the Au layer, since the emission source is quite localized. At  $4 \times 10^{13}$  W/cm<sup>2</sup>, x-ray emission should persist after laser burnthrough, since it originates in a broad region of the corona. For both intensities, the time-integrated x-ray emission decreases as the Au layer becomes thin enough to replace gold by (CH)<sub>x</sub> in the x-ray-emitting region during the laser pulse.

Experiments to study these phenomena were performed with use of the 0.35- $\mu$ m OMEGA multibeam laser facility.<sup>9</sup> The laser initially provided 250–300 J in six beams, and later 1600 J in all 24 beams, in a nominal  $\tau_L = 650$  ps FWHM pulse. To obtain good uniformity, the beams were focused beyond the target so that the beam edges were tangent to the initial surface. Illumination nonuniformities were  $\approx 50\%$  rms (with 2:1 large-scale variations) for six-beam irradiations, but only  $\approx 20\%$  rms for 24-beam experiments. Target and irradiation configurations are summarized in Table II. Targets consisted of solid (CH)<sub>x</sub> spheres coated with a layer of gold. We used a series of targets with different Au thicknesses (0.01–0.4  $\mu$ m) which bracketed the predicted midpulse laser penetration depth, as well as thick-Au

targets (1.5–3  $\mu$ m), essentially equivalent to solid gold spheres. Gold thicknesses were determined to be uniform to 10% (at all thicknesses) by scanning-electron-microscope analysis.

Target behavior was observed with use of a large array of diagnostics. The absorbed energy was measured to about 10% accuracy with 20 plasma calorimeters. Measured absorptions were 85%–95%, 70%–80%, and 55%–60% (calculations without refraction obtain 100%, 100%, 44%) at  $4 \times 10^{13}$  or below,  $4 \times 10^{14}$ , and  $4 \times 10^{15}$  W/cm<sup>2</sup>, respectively. Absolute x-ray emission measurements were obtained with a four-channel Al-photocathode x-ray diode (XRD) spectrometer covering 0.1–2 keV with 300-ps time resolution.<sup>10</sup> An x-ray transmission-grating/streak-camera spectrograph provided time-resolved (15 ps) spectra from 0.5 to 3 keV. For the 24-beam experiments, a time-integrating transmission grating spectrograph provided 0.1–3-keV spectra with  $\approx 2$  Å resolution. X-ray microscopes imaged the plasma's kiloelectronvolt emission.  $M$ - and  $N$ -line emission spectra<sup>11</sup> were studied with time-integrated and time-resolved<sup>12</sup> crystal spectrographs. Gold  $M$ -line emission (near 2.5 keV) was present above  $10^{14}$  W/cm<sup>2</sup> and absent at lower intensities, as predicted. The hard-x-ray bremsstrahlung (10–100 keV) was measured and implied negligible levels of instability-produced superhot electrons ( $< 10^{-4} E_{\text{laser}}$ ).

Soft-x-ray conversion efficiencies ( $h\nu < 2$  keV) were inferred from least-squares fits to the XRD signals, with use of the XRD response functions convolved with a spectral shape obtained either from the time-integrated grating-spectrograph measurements or from LASNEX calculations. We found that the results are insensitive to the differences between the measured and calculated spectra for the relatively broad-band subkiloelectronvolt responses used here: The conversion efficiencies obtained with use of the two types of spectra agree to within 10%. For the same reason, we estimate that Au  $M$ -line emission, which might spuriously increase the inferred x-ray conversion efficiencies, had little effect.

The conversion efficiencies for thick gold layers are shown in Fig. 1, together with LASNEX predictions assuming  $f_e = 0.08$  ( $f_e = 0.03$  is also shown, as used in the analysis of previous experiments<sup>2</sup>). The six-beam data exhibit no intensity dependence and agree well with the previous 0.35- $\mu$ m plane-target data<sup>2</sup> (but disagree with calculations). Thus, the planar results were apparently not much affected by 2D effects. In contrast, the 24-beam data show a significant intensity dependence and good agreement with LASNEX calculations with use of  $f_e = 0.08$ . Thus, for the 24-beam experiments, the overall energy balance appears to be roughly as calculated. A single broad-band (0.15–2 keV) XRD channel showed no intensity dependence in the six-beam series, and distinct intensity dependence in the 24-beam series. Thus, the difference between the two irradiation classes

TABLE II. Target and irradiation configurations.

Intensity (W/cm <sup>2</sup> )	Number of beams	Energy (J)	Target $D$ ( $\mu$ m)
$5 \times 10^{12}$	24	250	1650
$4 \times 10^{13}$	6,24	250,1800	600,1600
$4 \times 10^{14}$	6,24	250,1700	200,450
$3 \times 10^{15}$	24	1600	140

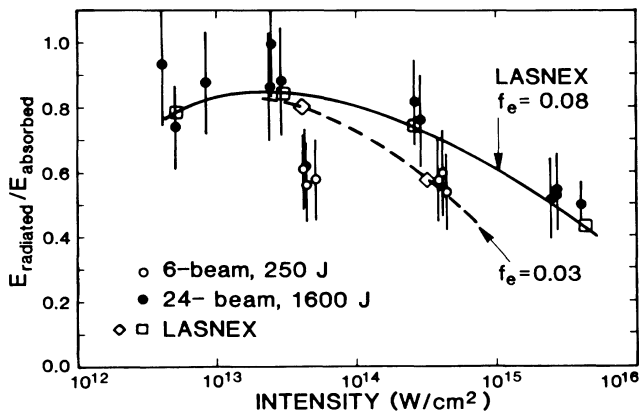


FIG. 1. X-ray conversion efficiencies inferred from spherical targets.

is not an artifact of the analysis. This difference suggests target-size or energy dependence (possibly due to changes in plasma scale length or optical depth of the emitting region) or perhaps dependence upon illumination uniformity.<sup>6,7</sup> Since the cause of these changes is not well understood, continued study is needed. We note that recent plane-target measurements at kilojoule energies<sup>13</sup> also show intensity dependence similar to our 24-beam results.

Figure 2 shows the relative conversion efficiency versus gold thickness for the 6- and 24-beam series, along with calculations using  $f_e = 0.08$ . As discussed above, when

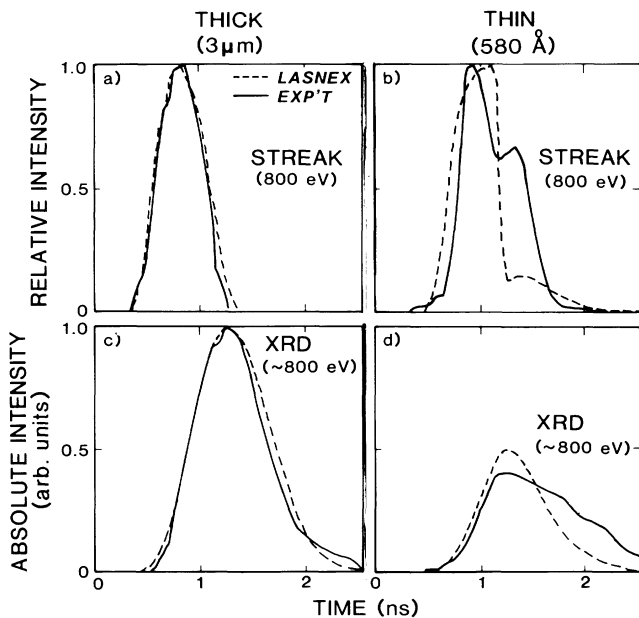


FIG. 2. X-ray conversion efficiency, normalized to the thick-Au values, as a function of gold-coating thickness.

the Au-layer thickness is reduced enough,  $(CH)_x$  replaces Au in the emission region during the laser pulse, and the time-integrated x-ray emission decreases. The rate of falloff depends upon both the rate of energy penetration and the relative localization of the x-ray emission. The general agreement in conversion efficiency falloff between the calculations and the data indicates that the energy penetration and x-ray-emission localization are well modeled. In particular, the penetration depth for both experimental series increases dramatically with increasing intensity. However, it is interesting to note that the more uniformly irradiated 24-beam targets show somewhat less rapid emission rolloff and poorer agreement with calculations, especially at  $4 \times 10^{14}$  W/cm<sup>2</sup> (see time-resolved measurements below). For both series at  $4 \times 10^{14}$  W/cm<sup>2</sup>, observations of CVI Lyman- $\alpha$  emission for Au thicknesses of  $\approx 750$  Å or less confirm the penetration of energy into the  $(CH)_x$ .

The time history of emission from the 24-beam experiment shows most of the burn-through features discussed above. Figure 3 shows measured and calculated emission pulses for thick and thin gold layers at  $4 \times 10^{14}$  W/cm<sup>2</sup>. We observed an abrupt emission decrease in the *N*-line region (near 800 eV) for thin targets, at the time predicted [Figs. 3(a) and 3(b)], indicating that the Au-layer burnthrough occurs as expected, consistent with a narrow emission region. No such abrupt reduction in emission for thin Au layers was seen at lower intensities, consistent with the expected broad emission region. We also observed a reduction in the absolute peak emission power for thin targets which agrees well with that calculated [Figs. 3(c) and 3(d)]. However, our measurements indicate that the magnitude of the emission decreases after burnthrough [Figs. 3(b) and 3(d)] is less than that predicted, perhaps indicating relatively greater emission from the underdense plasma than calculated. This excess late-time emission may be the cause of the slower rolloff in the 24-beam burnthrough curves at  $4 \times 10^{14}$  W/cm<sup>2</sup> (Fig. 2). We found that the burnthrough had little effect on the *M*-line region of the spectrum, as ex-

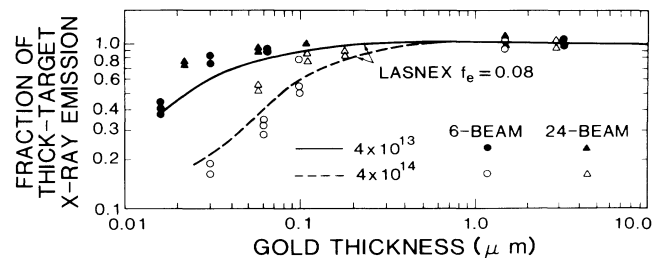


FIG. 3. X-ray emission pulses for thick and thin targets in the spectral regions of the gold *N* lines ( $\approx 800$  eV) for  $4 \times 10^{14}$  W/cm<sup>2</sup> irradiations. Time resolution was  $\approx 15$  ps for streaked data (a) and (b), and  $\approx 300$  ps for XRD data (c) and (d). XRD data and calculations are shown with the same arbitrary units.

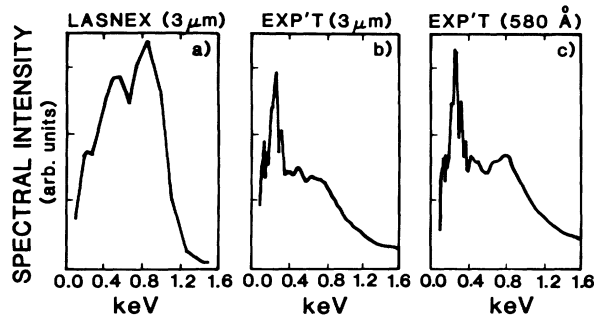


FIG. 4. X-ray spectra for Au-coated spheres (thickness as indicated), calculated and measured, at  $4 \times 10^{14}$  W/cm<sup>2</sup>. Vertical scale is linear.

pected, since this emission is generated primarily in the hot coronal plasma.

Grating spectrograph data for 24-beam irradiations show spectral details differing significantly from the calculations: The emission near 250 eV is considerably stronger than calculated relative to the 400–800-eV emission (Fig. 4). This again suggests that some details of the emission processes are not correctly modeled. However, the observed centroid of the *N*-band emission shifts from about 400 eV at  $4 \times 10^{12}$  W/cm<sup>2</sup> to about 800 eV at  $4 \times 10^{15}$  W/cm<sup>2</sup> as the mean charge state of the emitting region increases, as expected for warmer plasmas, and in agreement with calculations.

Images of kilovolt x-ray emission show limb brightening which corresponds in radial extent and relative brightness with calculations. The images also show small-scale spatial modulation of the emission, particularly for thin Au layers, which might be caused by filamentation<sup>14</sup> enhancing laser beam nonuniformities. However, we find no evidence that this affects the burnthrough or other plasma processes.

We find that the total soft-x-ray conversion efficiencies in the small-target irradiations agree with previous planar experiments and are intensity independent. The large-target results are intensity-dependent and in overall agreement with LASNEX calculations using near-classical thermal electron transport. Measurements of conversion efficiency and time dependence of emission for thin Au layers, and corroborating observations, indicate that the plasma flow and the energy-penetration and x-ray-emission depths are generally well understood. However, the emission spectra and certain details of the burnthrough time signatures are not reproduced by the calculations. Furthermore, the apparent dependence of x-ray emission upon target size, energy, or illumination uniformity is also not reproduced. Since the hydrodynamics and gross spatial aspects of the subkiloelectronvolt emission region are well calculated, it appears likely that these discrepancies originate in the atomic-

radiation-physics modeling. The approximations of the current non-local-thermodynamic-equilibrium atomic-physics model, including average-atom hydrogenic energy levels and rates, and neglect of subshell splitting, need to be examined further.

The authors thank the operations and target fabrication teams for their contributions to this work. The support of J. Browne, D. Cartwright, R. McCrory, and J. Soures is appreciated, as are discussions with R. Kauffman, B. Lasinski, J. Delettrez, and L. Suter. This work was supported by the U.S. Department of Energy (Office of Inertial Fusion), and by the University of Rochester Laser Fusion Feasibility Project.

<sup>1</sup>H. Nishimura *et al.*, Phys. Fluids **26**, 1688 (1983).

<sup>2</sup>W. C. Mead *et al.*, Phys. Fluids **26**, 2316 (1983); R. E. Turner *et al.*, Lawrence Livermore National Laboratory Report No. UCRL-50021-81, 1982 (unpublished), pp. 6-34 to 6-35.

<sup>3</sup>R. Kodama *et al.*, J. Appl. Phys. **59**, 3050 (1986); T. Mochizuki *et al.*, Phys. Rev. A **33**, 525 (1986).

<sup>4</sup>J. H. Nuckolls, Lawrence Livermore National Laboratory Report No. UCRL-50021-80, 1981 (unpublished), pp. 3-1 to 3-3; S. R. Goldman and W. C. Mead, Nucl. Fusion **26**, 813 (1986).

<sup>5</sup>G. B. Zimmerman, Lawrence Livermore National Laboratory Report No. UCRL-75881, 1974 (unpublished); G. B. Zimmerman and W. L. Kruer, Comments Plasma Phys. Controlled Fusion **2**, 51 (1975); R. M. More and G. B. Zimmerman, Lawrence Livermore National Laboratory Report No. UCRL-500-21-79, 1980 (unpublished), p. 3-66.

<sup>6</sup>Differences between planar and spherical geometries are conceivable, since thermal transport in low-*Z* plasmas behaves differently in the two classes of experiments; cf. B. Yaakobi *et al.*, Opt. Commun. **39**, 175 (1981); B. Yaakobi *et al.*, Phys. Fluids **27**, 516 (1984); W. C. Mead *et al.*, Phys. Fluids **27**, 1301 (1984), and references therein.

<sup>7</sup>A. Hauer *et al.*, Phys. Rev. Lett. **53**, 2563 (1984).

<sup>8</sup>M. D. Rosen, *et al.*, Phys. Fluids **22**, 2020 (1979).

<sup>9</sup>J. M. Soures *et al.*, in *Proceedings of the Tenth Symposium on Fusion Engineering*, Philadelphia, PA, 1983, edited by C. C. Hopkins, D. M. Pulyer, J. N. Stacy, and K. E. Wakefield (IEEE, New York, 1983), p. 1392.

<sup>10</sup>G. Pien *et al.*, Nucl. Instrum. Methods **B18**, 101 (1986).

<sup>11</sup>Laboratory for Laser Energetics (Univ. of Rochester) Review, 1965 (unpublished), Vol. 22, p. 60; M. C. Richardson *et al.*, to be published.

<sup>12</sup>B. L. Henke and P. Jaanimagi, Rev. Sci. Instrum. **56**, 1597 (1985).

<sup>13</sup>R. L. Kauffman *et al.*, Bull. Am. Phys. Soc. **29**, 1183 (1984).

<sup>14</sup>O. Willi and P. T. Rumsby, Opt. Commun. **37**, 45 (1981); M. J. Herbst *et al.*, Phys. Rev. Lett. **46**, 328 (1981); R. S. Craxton and R. L. McCrory, J. Appl. Phys. **56**, 108 (1984); K. G. Estabrook, W. L. Kruer, and D. S. Bailey, Phys. Fluids **28**, 19 (1985).